JACS
JOURNAL OF THE AMERICAN CHEMICAL SOCIETY

ARTICLE

pubs.acs.org/JACS

A Redox Series of Aluminum Complexes: Characterization of Four Oxidation States Including a Ligand Biradical State Stabilized via Exchange Coupling

Thomas W. Myers,[†] Nasrin Kazem,[†] Stefan Stoll, R. David Britt, Maheswaran Shanmugam, and Louise A. Berben*

Department of Chemistry, University of California, Davis, California 95616, United States

Supporting Information

ABSTRACT: Electrophilic activation and subsequent reduction of substrates is in general not possible because highly Lewis acidic metals lack access to multiple redox states. Herein, we demonstrate that transition metal-like redox processes and electronic structure and magnetic properties can be imparted to aluminum(III). Bis(iminopyridine) complexes containing neutral, monoanionic, and dianionic iminopyridine ligands (IP) have been characterized structurally and electronically; yellow (IP)$AlCl_3$ (**1**), deep green $(IP^-)_2AlCl$ (**2**) and $(IP^-)_2Al(CF_3SO_3)$ (**3**), and deep purple $[(IP^{2-})Al]^-$ (**5**) are presented. The mixed-valent, monoradical complex $(IP^-)(IP^{2-})Al$ is unstable toward C−C coupling, and $[(IP^{2-})Al]^{2-}$ (μ-IP−IP)$^{2-}$ (**4**) has been isolated. Variable-temperature magnetic susceptibility and EPR spectroscopy measurements indicate that the biradical character of the ligand-based triplet in **2** is stabilized by strong antiferromagnetic exchange coupling mediated by aluminum(III): $J = -230\ cm^{-1}$ for $\hat{H} = -2J(\hat{S}_{L(1)} \cdot \hat{S}_{L(2)})$. Coordination geometry-dependent $(IP^-)-(IP^-)$ communication through aluminum(III) is observed electrochemically. The cyclic voltammogram of trigonal bipyramidal **2** displays successive ligand-based oxidation events for the two $IP^{1-/0}$ processes, at −0.86 and −1.20 V vs SCE. The 0.34 V spacing between redox couples corresponds to a conproportionation constant of $K_c = 10^{5.8}$ for the process $(IP^-)_2AlCl + (IP)_2AlCl \rightarrow 2(IP^-)(IP)AlCl$ consistent with Robin and Day Class II mixed-valent behavior. Tetrahedral **5** displays localized, Class I behavior as indicated by closely spaced redox couples. Furthermore, CV's of **2** and **5** indicate that changes in the coordination environment of the aluminum center shift the potentials for the $IP^{1-/0}$ and $IP^{2-/1-}$ redox couples by up to 0.9 V.

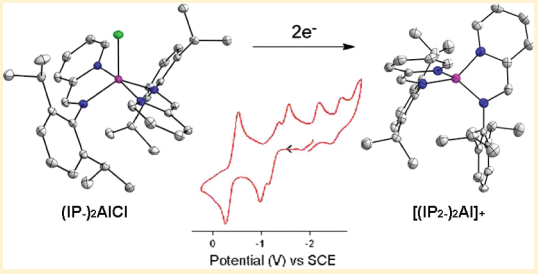

INTRODUCTION

A defining characteristic of transition metal reactivity is the ability of these metal centers to effect the activation and subsequent redox transformations of substrates.[1] It is also known that moderately Lewis acidic ions such as the alkali or alkaline earth metal ions, late transition ions Cu(I/II) or Zn(II), or highly electrophilic main group metal centers such as Al(III) can facilitate substrate activation.[2] However, following substrate activation, subsequent redox chemistry is in general not possible without addition of a sacrificial oxidant or reductant, and so the investigation of redox activity, redox transformations, or electrocatalytic reactions of substrates by Lewis acidic metal complexes is not well-known. Herein, we use redox-active ligands to demonstrate that transition metal-like redox processes and electronic structure and magnetic properties can be imparted to aluminum(III) complexes.

Recent work in main group chemistry concerning, for example, catalytic hydrogenation,[3] or activation of ethylene,[4] has demonstrated that transition metal-like reactivity can be observed. In the context of small molecule chemistry, some examples of Lewis acid-assisted activation are known for CO_2 activation. For example, addition of alkali metal ions to systems employing redox-active transition metal electrocatalysts has been shown to facilitate CO_2 binding and reduction at lower energies relative to transition metal-only catalyst systems.[5−7] In another example, highly electrophilic aluminum trichloride has been shown to coactivate CO_2 to yield isolable species such as $AlCl_3 \cdot CO_2 \cdot PMes_3$, for which the solid-state structure was characterized crystallographically.[8] However, to effect redox transformations at the immobilized CO_2 molecule, external redox reagents must be employed, and hence only stoichiometric transformations are possible; for example, the sacrificial hydride donor ammonia borane in combination with water could be used to effect reduction of CO_2 to MeOH from $AlCl_3 \cdot CO_2 \cdot PMes_3$.[8]

Highly Lewis acidic aluminum is the most abundant metallic element on earth, comprising 7−8% of the earth's crust and as such is an appealing element for use in large-scale applications including catalysis. Aluminum is commonly found only in the +3 oxidation state, and so facile redox transformations of small molecules are not possible. Aluminum can be rendered redox-active by employing a very harsh reducing agent such as potassium metal and a ligand, which enforces a low coordination number.

Received: February 28, 2011
Published: May 13, 2011

dx.doi.org/10.1021/ja2015718 | J. Am. Chem. Soc. 2011, 133, 8662–8672

Chart 1. Structures of Ligands Mentioned in the Text with Their Abbreviations

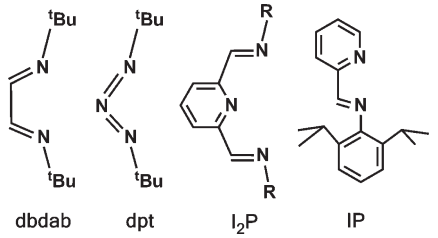

For instance, using low-valent aluminum synthons, Roesky and co-workers have reported two-electron oxidation reactions involving an Al(I) to Al(III) transformation.[9,10] These impressive, albeit isolated cases further illustrate the difficulty of using aluminum for facile and tunable redox chemistry. To investigate the possibility of facile redox transformations via electrophilic activation at an aluminum metal center, we are exploring the chemistry of aluminum(III) complexes with redox-active ligands: in principle, an aluminum complex of the form $(L)_2AlX$ (L = redox active ligand) could give access to five successive redox states if each ligand L can access three oxidation states, for example, L, L^-, and L^{2-}. In addition, by judicious choice of redox-active ligand, these redox states could be accessed at a wide range of potentials, some of which may be very mild and allow careful control of reactivity.

The majority of paramagnetic and potentially redox-active aluminum(III) complexes feature N-donor ligands (Chart 1), and, in general, a detailed understanding of their structural properties, redox chemistry, and electronic and magnetic properties has not been elucidated. The earliest reported, redox-active and paramagnetic complex of aluminum(III) was $Al(bpy)_3$ (bpy = 2,2′-bipyridyl).[11] On the basis of the magnetic moment of the complex, it was suggested that it is best described as an Al^{3+} cation, with the unpaired electrons extensively delocalized on the bpy ligands as three radical anions. The reported magnetic moment for $Al(bpy)_3$, of 2.32 μ_B is lower than expected, for three unpaired electrons, and suggests that some antiferromagnetic coupling through aluminum is present. Subsequent work by Kaim and others resulted in the isolation of related dialkyl Al(III) complexes of the pyrazine, pyridine, and bipyridine radical anions.[12,13] Raston and co-workers studied the reactivity of alanes and aluminum metal with dbdab (dbdab = 1,4-di-*tert*-butyl-1,4-diazabutadiene) resulting in the isolation of $Al(dbdab)_2$ and partially hydrogenated $Al(dbdab)(dbdabH_2)$.[14] The EPR spectrum of $Al(dbdab)_2$ shows hyperfine coupling to four equivalent nitrogen atoms but not to the aluminum nucleus, and thus the radical is most likely ligand centered and delocalized over both ligands on the EPR time scale. In a study reported by Barron and co-workers roughly 20 years ago, $Al(dpt)_3$ (where dpt = 1,3-diphenyltriazenido) was isolated and characterized.[15] Recently, substituted bis(imino)pyridine (denoted I_2P) complexes of aluminum(III) have been isolated. Richeson and co-workers have isolated a neutral ligand complex,[16] and Gambarotta and co-workers reported a reduced-ligand complex.[17]

In this work, we have undertaken the task to isolate bis(iminopyridine) aluminum(III) complexes of the form $(IP^{n-})Al-X$, in a wide range of oxidation states, and to thoroughly characterize the magnetic and electronic properties of these molecules. We find that five oxidation states can be observed electrochemically, and we have isolated four of these, which have $S = 0$ and $S = 1$ spin states at room temperature. We show that mixed-valent, doublet oxidation states are unstable toward radical coupling of the iminopyridine ligands and present evidence that stabilization of the biradical, triplet oxidation state at room temperature is due to strong electronic and magnetic interactions mediated by the aluminum(III) center between unpaired electrons on iminopyridine ligands. In fact, the ground state may be more accurately referred to as a singlet biradical state. We have also found that substitution at the aluminum center can shift the position of the ligand redox potentials by up to 0.9 V. Taken together, these results indicate that appropriately chosen redox-active ligand sets can impart magnetic and electronic properties reminiscent of the transition metals to complement the highly electrophilic properties of a main group element.

RESULTS AND DISCUSSION

Synthesis of Aluminum Complexes 1−6. Iminopyridine ligands and derivatives thereof have been employed as ligands for Mg^{2+},[18] with divalent ions of the first row transition series from Cr^{2+} to Zn^{2+},[19] and recently as ancillary ligands for Fe^{2+} complexes, which are active for catalysis of hydrosilylation reactions.[20] In the examples of paramagnetic aluminum complexes highlighted above, the metal center is most often coordinatively saturated by the redox-active ligands and has the form L_3Al (where L = bidentate ligand). In the present study, we focus on the (2,6-diisopropylphenyl)-substituted iminopyridine ligand because we find that its moderate size prevents formation of the L_3Al moiety and favors formation of four- and five-coordinate complexes of aluminum with open coordination sites: IP_2Al or IP_2AlX (where IP = 2,6-bis(1-methylethyl)-*N*-(2-pyridinylmethylene)phenylamine, and X is a monodentate ligand). In this work, all three oxidation states of the iminopyridine ligand can be stabilized at one metal center, and the doubly reduced ligand is isolated as a nonbridging ligand in a monomeric complex. We attribute both of these results to the stability of the bonding obtained by the interaction between highly charged Al^{3+} and strongly donating iminopyridine.

Using $AlCl_3$ as a starting reagent, control of the number of chloro ligands at the aluminum center in a series of product complexes was achieved by limiting the number of equivalents of Na used as reducing agent. We found that removal of chloride ion from the $AlCl_3$ coordination sphere as NaCl was necessary to drive the reactions and was dependent on the presence of Na^+ ions generated during ligand reduction by sodium metal. If no sodium is added to the reaction of $AlCl_3$ with neutral IP, the five-coordinate complex $IPAlCl_3$ (**1**) could be isolated. A summary of the preparation of complexes **2**−**5** is described in Scheme 1. A dark green aluminum(III) complex, $(IP^-)_2AlCl$ (**2**) in which the two IP ligands are each reduced by one electron, was prepared by combination of $AlCl_3$ with 2 equiv of IP and 2 equiv of sodium in 1,2-dimethoxyethane (DME). The corresponding triflate-substituted complex $(IP^-)_2Al(CF_3SO_3)$ (**3**) could be prepared from $Al(CF_3SO_3)_3$ in an analogous manner.

Synthesis of a mixed-valent, overall three-electron per aluminum center reduced complex, $(IP^-)(IP^{2-})Al$, was attempted. In this case, direct three-electron reduction of the constituent $AlCl_3$ and 2 equiv of IP using sodium, or reduction of **2** by 1 equiv of sodium metal, both resulted in a three-electron per aluminum reduced product. However, under both sets of reaction conditions, dimerization of the complexes through the ligand backbone

dx.doi.org/10.1021/ja2015718 |*J. Am. Chem. Soc.* 2011, 133, 8662–8672

Scheme 1. Synthesis of Aluminum Complexes 1−5

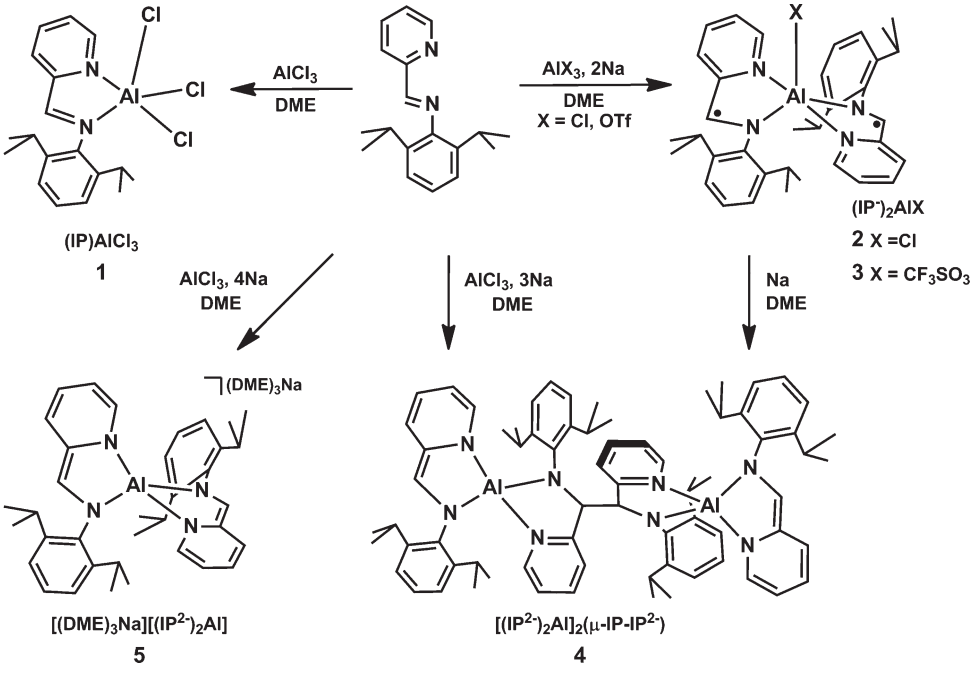

has occurred to yield $[(IP^{2-})Al]_2(IP-IP)^{2-}$ (**4**), preventing the formation of a monometallic aluminum complex. In **4**, each aluminum center is coordinated by a two-electron reduced and a one-electron reduced ligand; the one electron reduced ligand, IP^-, has undergone C−C coupling through the formerly imine carbon of IP. In addition to the metrics from single crystal X-ray studies (vide infra), this observed reactivity provides further evidence for the radical nature of the ligand IP^- upon one-electron reduction. It is interesting to note that for complexes **2** and **3**, in which each of the ligands are reduced by one electron, we have never observed evidence for dimerization via C−C coupling of the ligand. This reactivity difference suggests that the ligand radical of **2** and **3** is energetically stabilized with respect to the ligand radical of the one-electron reduced ligand generated during the synthesis of **4**. We propose that the stabilization of the ligand radicals in **2** and **3** is achieved by antiferromagnetic coupling of the unpaired electrons through the aluminum center, which reduces the effective unpaired spin density residing at the carbon atom of the imine functional group. Electrochemical and magnetic susceptibility evidence for coupling between the unpaired electrons is discussed below.

Preparation of a deep purple, overall four-electron reduced complex, $[(DME)_3Na][(IP^{2-})_2Al]$, **5**, in which two ligands are each reduced by two electrons was achieved by increasing the ratio of IP to Na up to 1:2.5. In this case, use of DME as a solvent was necessary to chelate the sodium countercation and prevent coordination of sodium to one of the anionic pyridine rings. When the reaction is performed in diethyl ether instead of DME, the sodium countercation was observed coordinated to a pyridine ring and two diethyl ether molecules in the solid-state structure: $[(Et_2O)_2Na][(IP^{2-})_2Al]$, **6**.

Compounds **1**−**6** are soluble in alkanes, aromatic, and ether solvents. The most reduced complexes, **5** and **6**, decompose in the presence of MeCN or dichloromethane. The NMR spectra of the neutral and four-electron reduced complexes **1**, **5**, and **6** are indicative of formation of a diamagnetic complex: peaks in the aromatic region are shifted as compared to the free ligand but remain sharp and consistent with chemical shifts located as expected. The NMR spectra of **2** and **3** display peaks broadened and shifted from the expected positions, which implies that in each case the complexes are paramagnetic at room temperature. Complexes **2** and **3** differ from each other only in the identity of the fifth ligand at the aluminum center, Cl^- or $CF_3SO_3^-$, respectively. Reflecting this similarity, many of the observed proton resonances have similar chemical shifts. For example, the proton resonances for the pyridine rings are observed at 8.6, 8.4, and 8.2 ± 0.1 ppm in each case. For compounds **4**−**6**, the NMR spectra provide further evidence that the reduction events involved in preparation of the complexes are localized on the ligands rather than the metal; as expected for a two-electron reduction per ligand, the observed chemical shifts corresponding to proton resonances on the pyridine rings do not fall within the expected range of aromatic proton resonances. For example, in **5**, four resonances for the formerly pyridine protons are observed in the range 5.91−4.65 ppm, as compared to the range of 8.16−7.63 ppm for the aromatic pyridine protons of the neutral ligand in **1**.

Consistent with the intense deep green and purple colors of **2**−**6**, the electronic absorption spectra obtained in hexanes solution display a series of intense absorption bands (Figures 1 and S1). The electronic configuration of Al(III) is [Ne], and so we attribute each of these absorption bands to ligand-based $\pi-\pi^*$ transitions. Similar assignments have been made for previously studied Zn^{2+} complexes of iminopyridine ligands.[19] The neutral free ligand, IP, displays one intense absorption at 370 nm (1500 L mol^{-1} cm^{-1}, Figure S1): this band increases in intensity to 2000 L mol^{-1} cm^{-1}, and shoulders extend further into the visible region as 1, followed by 2, equiv of sodium metal are added to effect reduction of IP. Upon coordination of the ligand to an aluminum center, this band increases significantly in intensity. In complexes **2**−**5**, a band at 370 nm is observed, which

dx.doi.org/10.1021/ja2015718 |*J. Am. Chem. Soc.* 2011, 133, 8662–8672

decreases in intensity (ca. 38 700 down to 5500 L mol^{-1} cm^{-1}) as the complex is successively reduced in one-electron steps starting from one electron reduced per ligand in **2**, down to two electrons per ligand in **5**. Further evidence for a ligand-based assignment is that the absorption spectra of complexes **2** and **3** in which the fifth coordination site on aluminum is occupied by a chloro or triflate, respectively, are almost identical to each other (Figure 1). In addition to the absorption at 370 nm, the dark green complexes, **2** and **3**, in which the ligands are each one-electron reduced, exhibit a broad and less intense transition (5000 L mol^{-1} cm^{-1}) at 700 nm attributed to $\pi-\pi^*$ transitions.

Solid-State Structures of 1−6. Single crystals of **1** were grown by diffusion of ether into MeCN. Each of the complexes

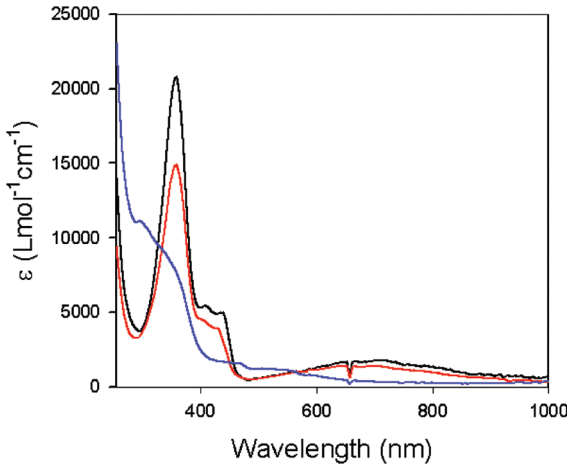

Figure 1. UV−visible absorption spectra of complexes **2** (black), **3** (red), and **5** (blue).

was grown by chilling concentrated solutions at −30 °C for about 1 week. Complexes **3**, **4**, and **5** were crystallized from DME, and complexes **2** and **6** were crystallized from diethyl ether (Table 1). The complexes are four or five coordinate and contain two iminopyridine ligands (Tables 2 and 3): the five-coordinate complexes contain an additional monodentate ligand. The five-coordinate complexes (**1**, **2**, and **3**) are best described as distorted trigonal pyramidal in geometry: τ values are all close to 1 (0.7151−0.8250) (Figures 2, S2, and S4).[21] For complex **1**, the Al−N_{py} and Al−Cl(3) bond vectors lie along the axial direction of the molecule, and the N_{py}−Al−Cl(3) bond angle is 168.19(13)°. In **2** and **3**, the Al−N_{py} and Al−$N_{py'}$ bond vectors lie along the axial direction, and the N_{py}−Al−$N_{py'}$ bond angles are 169.59(6)° and 176.49(5)° for **2** and **3**, respectively. The Al−N_{im}, Al−$N_{im'}$, and Al−X bonds (X = Cl, triflate in **2** and **3**, respectively) lie in the equatorial trigonal plane. The four-coordinate complexes, **4**−**6** are pseudo tetrahedral: the N_{im}−Al−N_{py} bite angles of each ligand are pinched as compared to perfect tetrahedral angles and range from 84.97(12)° for the one-electron reduced ligand in **3** to 89.47(1)°, 87.87(17)°, and 88.57(9)° for the two-electron reduced ligands in **4**−**6** (Figures 3, 4, and S4). Complementing these pinched angles, the interligand N−Al−N bond angles are more obtuse, ranging from 110.94(9)° in **6** to 134.47(13)° in **4**.

The bond distances and angles in the neutral ligand in complex **1** are unremarkable and serve as a reliable benchmark for comparison with the bond lengths and angles in the one- and two-electron reduced ligands in complexes **2**−**6** (Figure 5). In **2** and **3**, the bond lengths and angles of the iminopyridine ligands are consistent with reduction by one electron, and some general trends in bond lengths and angles associated with this reduction were observed. Metric parameters for **2** and **3** show the same general trends, and so only a detailed discussion of **2** is presented

Table 1. Crystallographic Data[a] for the Complexes (IP)$AlCl_3$·DME (1), (IP^-)$_2$AlCl (2), (IP^-)$_2$Al(CF_3SO_3)·DME (3), [(IP^{2-})$_2$$Al_2$]($\mu$-$IP^-IP^-$)·2$C_6H_6$ (4), [(DME)$_3$Na][(IP^{2-})$_2$Al]·0.5DME (5), and [(Et_2O)$_2$Na] (IP^{2-})$_2$Al (6)

	1	2	3	4	5	6
formula	$C_{22}H_{32}N_2O_2Cl_3$	$C_{36}H_{44}N_4AlCl$	$C_{41}H_{54}N_4AlF_3O_5S$	$C_{84}H_{100}N_8Al$	$C_{50}H_{75.25}N_4O_7AlNa$	$C_{44}H_{64}N_4O_2AlNa$
crystal size	0.15 × 0.10 × 0.08	0.17 × 0.12 × 0.08	0.45 × 0.43 × 0.41	0.35 × 0.29 × 0.17	0.10 × 0.08 × 0.06	0.29 × 0.26 × 0.19
formula weight, g mol^{-1}	489.83	595.18	798.92	1275.68	894.36	730.96
space group	$P2_1/n$	$P2_1/c$	$P2_1/c$	$P\bar{1}$	$P2_1/c$	$P2_1/c$
a, Å	17.558(3)	15.796(3)	13.568(5)	14.273(9)	13.862(5)	12.543(7)
b, Å	9.835(18)	9.918(2	18.277(7)	15.308(12)	16.958(4)	14.039(8)
c, Å	29.527(5)	21.960(4)	17.138(7)	19.838(12)	22.251(8)	24.0531(14)
α, deg	90	90	90	108.478(10)	90	90
β, deg	90.172(6)	110.01(3)	102.473(7)	99.313(10)	90.59(6)	97.574(10)
γ, deg	90	90	90	108.466(10)	90	90
V, Å^3	5098.5(16)	3232.8(11)	4149(3)	3730.1(4)	5231(3)	4198.3(4)
Z	8	4	4	2	4	4
T, K	100 (2)	100 (2)	100 (2)	100 (2)	100 (2)	100 (2)
ρ, calcd, g cm^{-3}	1.276	1.223	1.279	1.136	1.136	1.156
reflns collected/$2\theta_{max}$	47 377/52.04	80 818/58.88	47 376/61.28	41 246/50.06	33 537/42.98	49 333/56.56
unique reflns/ $I > 2\sigma(I)$	10 028/7208	8942/6893	12 082/9106	13 170/8337	5992/4522	10 407/6836
parameters/restraints	541/0	387/0	506/0	787/0	618/108	477/0
λ, Å/μ (Kα), cm^{-1}	0.71073/0.415	0.71073/0.177	0.71073/0.160	0.71073/0.088	0.71073/0.098	0.71073/0.099
R_1/GOF[b]	0.0641/1.060	0.0487/1.042	0.0405/1.052	0.0687/1.219	0.0739/1.019	0.0628/0.940
wR_2 ($I > 2\sigma(I)$)[b]	0.1685	0.1221	01412	0.2080	0.1953	0.1912
residual density, e Å^{-3}	+1.089/−0.353	+0.453/−0.274	+0.452/−0.381	+0.704/−0.436	+1.550/−0.832	+1.287/−0.511

[a] Obtained with graphite-monochromated Mo Kα (λ = 0.71073 Å) radiation. [b] $R_1 = \Sigma||F_o| - |F_c||/\Sigma|F_o|$, w$R_2 = \{\Sigma[w(F_o^2 - F_c^2)^2]/\Sigma[w(F_o^2)^2]\}^{1/2}$.

dx.doi.org/10.1021/ja2015718 |*J. Am. Chem. Soc.* 2011, 133, 8662–8672

Table 2. Selected Average Interatomic Distances (Å) for the Complexes in $(IP)AlCl_3 \cdot DME$ (1), $(IP^-)_2AlCl$ (2), $(IP^-)_2Al(CF_3SO_3) \cdot DME$ (3), $[(IP^{2-})_2Al_2](\mu\text{-}IP^-IP^-) \cdot 2C_6H_6$ (4), $[(DME)_3Na][(IP^{2-})_2Al] \cdot 0.5DME$ (5), and $[(Et_2O)_2Na](IP^{2-})_2Al$ (6)

	$Al-N_{im}$	$Al-N_{py}$	$Al-X^a$	$C_{im}-N_{im}$	$C_{im}-C_{py}$	$C_{py}-N_{py}$	$C_{py}-C(3)$
1	2.038(4)	2.084(4)	2.1847(19)	1.284(6)	1.453(7)	1.347(6)	1.391(6)
2	1.915(14)	2.009(15)	2.191(1)	1.354(2)	1.405(2)	1.366(2)	1.412(2)
3	1.893(12)	1.981(13)	1.857(12)	1.375(17)	1.427(17)	1.358(16)	1.405(18)
4	1.824(3),[b] 1.833(2)[c]	1.851(3),[b] 1.937(2)[c]	na	1.411(4),[b] 1.478 (4)[c]	1.344(5),[b] 1.520(4)[c]	1.401(4),[b] 1.350(4)[c]	1.412(2),[b] 1.384(4)[c]
5	1.844(4)	1.873(4)	na	1.414(6)	1.356(6)	1.399(6)	1.437(6)
6[d]	1.852(2)	1.858(2)	na	1.413(3)	1.355(3)	1.401(3)	1.442(3)

[a] X = Cl or O. [b] Two-electron reduced L. [c] One-electron reduced L. [d] Data not included for pyridine ring, which is coordinated to Na^+.

Table 3. Selected Average Angles (deg) for the Complexes in $(IP)AlCl_3 \cdot DME$ (1), $(IP^-)_2AlCl$ (2), $(IP^-)_2Al(CF_3SO_3) \cdot DME$ (3), $[(IP^{2-})_2Al_2](\mu\text{-}IP^-IP^-) \cdot 2C_6H_6$ (4), $[(DME)_3Na][(IP^{2-})_2Al] \cdot 0.5DME$ (5), and $[(Et_2O)_2Na]$ $(IP^{2-})_2Al$ (6)

	τ^a	$N_{im}-Al-N_{py}$	$N_{py}-Al-N_{im'}$	$N_{im}-Al-N_{im'}$	$N_{py}-Al-N_{py'}$
1	0.8250	77.39(16)	n/a	n/a	n/a
2	0.8180	81.46(6)	93.85(6), 93.61(6)	125.28(6)	169.59(6)
3	0.8175	82.87(5)	94.76(5), 96.50(5)	127.44(5)	176.49(5)
4		84.97(12),[c] 89.47(11)[b]	134.47(13), 123.99(14), 131.27(12), 112.24(12)	123.55(12), 129.99(13)	103.86(13), 105.96(11)
5		87.87(17)	125.87(18), 124.14(17)	122.26(18)	112.50(18)
6[d]		88.57(9)	126.49(10), 129.39(9)	118.69(9)	110.94(9)

	$X-Al-N_{im}$	$X-Al-N_{py}$	Cl−Al−Cl	$C_{py}-C_{im}-N_{im}$
1	118.12(13), 120.34(13)	89.45(13), 86.38(12)	118.70(8), 99.33(7)	117.7(4)
	91.36(12)	168.19(13)	99.16(7)	
2	117.87(5), 116.85(5)	95.21(5), 95.20(5)	n/a	116.73(14)
3	115.88(5), 116.59(5)	89.55(6), 93.84(6)	n/a	115.11(11)
4	n/a	n/a	n/a	118.1(3),[b] 107.1(2)[c]
5	n/a	n/a	n/a	117.1(4)
6	n/a	n/a	n/a	117.1(2)

[a] τ values calculated for five-coordinate complexes. [b] Ligand reduced by two electrons. [c] Ligand reduced by one electron. [d] Data not included for pyridine ring, which is coordinated to Na^+.

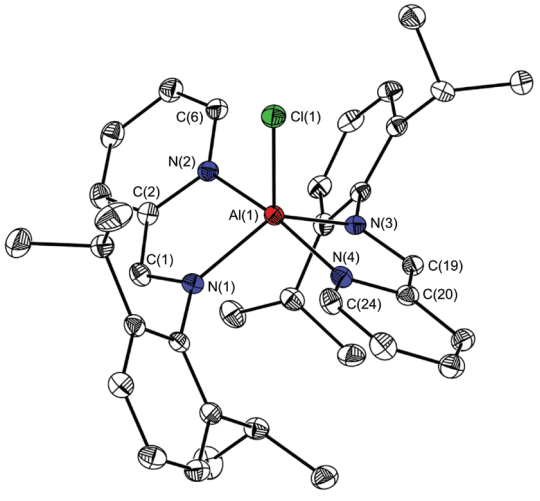

Figure 2. Structure of $(IP^-)_2AlCl$, **2**, in which the iminopyridine ligands are reduced by one electron each. Red, blue, and green ellipsoids represent Al, N, and Cl atoms, respectively; ellipsoids are shown at the 40% probability level, and H atoms are omitted for clarity.

here. In the aluminum(III) coordination sphere of **2**, the $N_{im}-Al(1)-N_{im'}$ bite angle has widened upon reduction from 77.47(16)° in **1** to 87.59(6)° in **2**. Consistent with partial localization of the negative charge on the imine nitrogen donor, shortening of the $Al-N_{im}$ bond, as compared to the bond in complex **1**, by 0.185 Å to 1.913(1) Å is observed. Shortening of the $Al-N_{im}$ bond is accompanied by other bond length changes within the ligand framework consistent with reduction localized on the imine functionality: the formerly C═N double bond lengthens from 1.284(6) to 1.352(2) Å, and the carbon-to-pyridine single bond, C(1)−C(2) in Figure 2, shortens to 1.405(6) Å. The pyridine ring largely retains aromatic character, and the bond lengths and angles deviate only very slightly from those in **1**.

In the ligand-based mixed-valent complex **4**, two aluminum (III) centers each have a local pseudotetrahedral coordination environment and are bridged by iminopyridine ligands that have dimerized. A C−C bond is formed by coupling of the ligand radicals formed when IP is reduced by one electron (Scheme 1). Comparison of the one-electron reduced and dimerized ligand in **4** with the one-electron reduced ligands in **2** reveals that dimerization further exaggerates the bond length changes associated with the imine functional group upon one-electron

dx.doi.org/10.1021/ja2015718 |*J. Am. Chem. Soc.* 2011, 133, 8662–8672

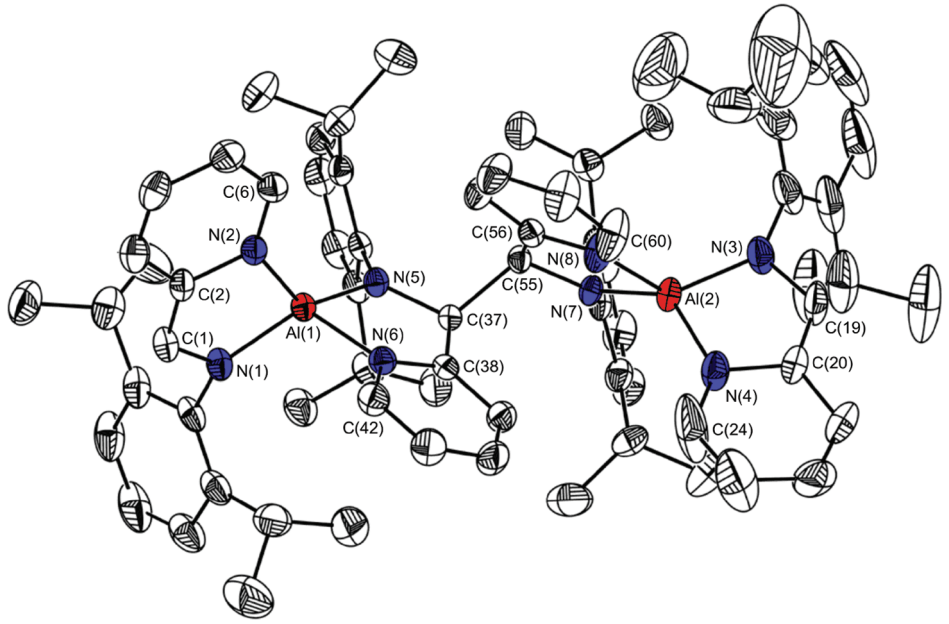

Figure 3. Structure of $[(IP^{2-})_2Al](L-L)$, **4**. Red and blue ellipsoids represent Al and N atoms, respectively; ellipsoids are shown at the 40% probability level, and H atoms are omitted for clarity.

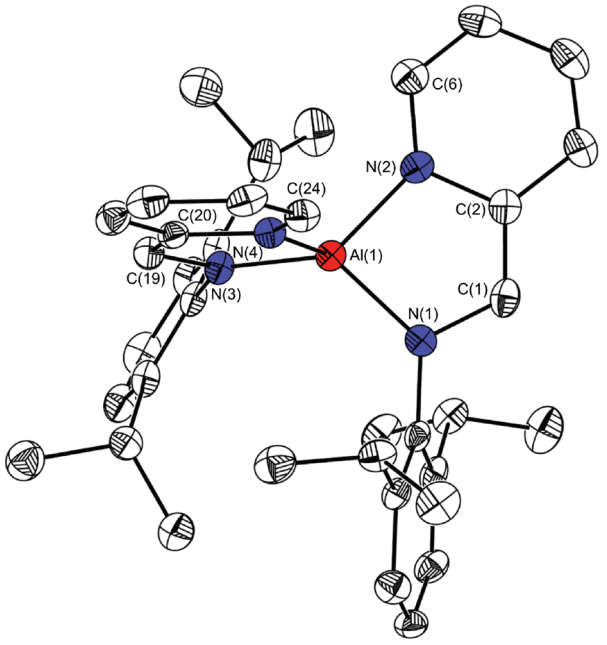

Figure 4. Structure of the anionic complex $[(IP^{2-})_2Al]^-$ in **5**. Red and blue ellipsoids represent Al and N atoms, respectively; ellipsoids are shown at the 40% probability level, and H atoms are omitted for clarity.

reduction; as expected, dimerization localizes the position of the reduction site at the carbon of the imine functional group. The formerly C═N double bond lengthens completely to a single bond at 1.478(4) Å. Unlike in **2** and **3**, the $C_{im}-C_{py}$ bond, C(37)−C(38) in **5**, retains single bond character due to formation of the new C−C bond via radical coupling.

Single crystals of a tetrahedral aluminum complex in which each ligand is reduced by two electrons could be isolated from reactions performed in DME. The negative charge on complex **5** is balanced by a sodium countercation chelated by three DME ligands. As mentioned above, the deviation from ideal tetrahedral geometry in this structure results from pinched chelate bite angles in the iminopyridine ligand. An almost 5° increase in bite angle was observed on going from the neutral ligand in **1** to the one-electron reduced ligand in **2**. In the two-electron reduced ligand in **5**, we observe roughly a further 5° increase in the $N_{im}-Al-N_{py}$ bite angle as compared to complex **2**. $Al-N_{im}$ and $Al-N_{py}$ bond lengths contract by 0.225 and 0.258 Å, respectively, as compared to the neutral ligand in **1**, which is consistent with the dianionic character of the two-electron reduced ligand. Internal ligand bond lengths in **5** show features consistent with a two-electron reduction per ligand. The formerly imine $C-N_{im}$ bond lengthens further to 1.414(4) Å, and the formerly carbon−pyridine bond C(2)−C(6) shortens to 1.356(6) Å. The alternating bond lengths in the formerly pyridine ring reflect a loss of aromaticity upon two electron reduction; the bond lengths observed, listed starting at the N_{py} atom, are 1.429(6), 1.437(6), 1.346(6), 1.440(6), 1.350(7), and 1.370(2) Å. In addition to the evidence provided by the alternating bond lengths in the pyridine ring, the anionic, and therefore nonaromatic character of the pyridine ring, is verified by the solid-state structure of complex **6**. Preparation of **6** was achieved by reaction and crystallization in the absence of the chelating DME solvent, which was effective to separate the Na^+ countercation from the anionic complex in **5**. With ether as the solvent for preparation of **6**, the sodium countercation is observed bound to the face of one of the anionic, (formerly) pyridine rings (Figure S4).

Further confirmation that the reduction events are localized at the ligands rather than the metal comes from comparison with the bond lengths reported for the handful of known iminopyridine complexes (Table 4). For the first row transition metal series reported by Wieghardt and co-workers, average distances of the C−C and $C-N_{imine}$ bond lengths in the one-electron reduced ligand are 1.409(5) and 1.340(5) Å, respectively. In complexes **2**−**4**, we find averages of 1.410(8) and 1.350(6) Å, respectively, which are in close agreement with those previously reported. The $C-N_{py}$ bond lengths are not noticeably affected

dx.doi.org/10.1021/ja2015718 |*J. Am. Chem. Soc.* 2011, 133, 8662–8672

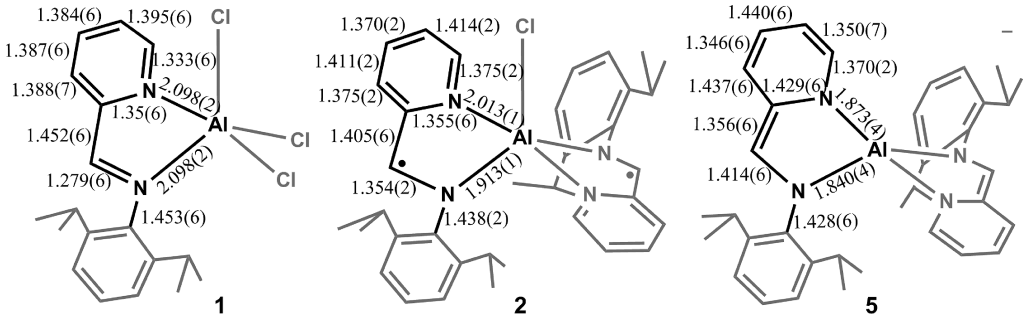

Figure 5. Comparison of bond lengths in complexes **1**, **2**, and **5**; the ligand oxidation states are IP, IP^{-}, and IP^{2-}, respectively.

Table 4. Comparison of Ligand Backbone Bond Lengths for One-Electron[19] and Two-Electron[22] Reduced Ligands from This Work with Values Reported in the Literature[a]

		literature (Å)	current work (Å)
IP^{-}	C−C	1.409(5)	1.410(8)
	$C-N_{im}$	1.340(5)	1.350(6)
IP^{2-}	C−C	1.366(6)	1.356(6)
	$C-N_{im}$	1.459(4)	1.414(4)
	$C-N_{py}$	1.404(4)	1.429(4)

[a] $C-N_{py}$ bond lengths do not change upon one-electron reduction and so were not included for this oxidation state.

by one-electron reduction of the ligand. For the two-electron reduced ligand, we found only one other set of data reported in the literature, and this corresponds to a complex in which the originally imine N atom bridges two magnesium centers.[22] In this case, the bond lengths for the ligand backbone, $C-N_{im}$, $C_{im}-C_{py}$, and $C_{py}-N_{py}$, were given as 1.366(6), 1.459(4), and 1.404(4) Å, respectively. These are in close agreement with the average bond lengths of the two independent ligands we observe in complex **5**: 1.356(6), 1.414(4), and 1.429(4) Å, respectively.

Electronic Structure. Magnetic susceptibility measurements were performed on complexes **2**, **4**, and **5** (Figures 6 and S5). Measurements were performed on multiple batches of all samples discussed and gave consistent results. Data were collected in an applied field of 1 T between 4 and 300 K. As expected, complexes **4** and **5** are diamagnetic. The observed magnetic moment at 300 K for complex **2** is 2.7 μ_B, which is consistent with the presence of an unpaired electron on each of the iminopyridine ligands, and with the apparent paramagnetism implied by the proton NMR spectrum of **2**. Temperature-dependent susceptibility measurements indicate that the magnetic moment falls steadily from 2.7 μ_B to 0.39 μ_B as the temperature is lowered from 300 to 4 K, consistent with strong antiferromagnetic coupling between the ligand radicals. The data were fit using MAGFIT3.0 and assuming a spin Hamiltonian of the form $\hat{H} = -2J\hat{S}_{L(1)} \cdot \hat{S}_{L(2)}$ and a value of $g = 2.0$; a value for the exchange coupling of $J = -230$ cm^{-1} was obtained.[23] A contribution from temperature-independent paramagnetism (TIP) was also observed: 2×10^{-3} emu.

In a previous report by Heyduk and co-workers, the observed increase in magnetic susceptibility with temperature for a ligand-based biradical system was modeled using purely a significant contribution from TIP: 945×10^{-6} emu.[24] This interaction was attributed to through-space coupling, rather than a metal-mediated phenomenon; the unpaired electrons were located on coplanar aryl rings situated only 3.4 Å apart. In the present example, we estimate, on the basis of the solid-state X-ray diffraction data and EPR spectroscopy measurements (vide infra), that the unpaired spins are located ∼5 Å apart and are canted roughly 120° with respect to each other. It seems unlikely that through-space coupling could be responsible for the observed strong antiferromagnetic coupling, and we propose that it is most likely a result of an aluminum-mediated superexchange pathway through empty 3p orbitals on Al(III). Strong superexchange through unfilled cyanide π^* orbitals or filled 2p orbitals of the isoelectronic O^{2-} ion is well-documented.[25] We are not aware of prior investigations in which a superexchange pathway through Al(III) is proposed.

EPR spectroscopy measurements confirm the ligand-based biradical, and the antiferromagnetic coupling at low temperature proposed for **2** based on variable temperature magnetic susceptibility measurements. The 100 K X-band continuous wave (cw) EPR spectrum of a dilute frozen solution of **2** features a pattern consisting of four lines between 310 and 360 mT characteristic of a triplet state ($S = 1$) as well as a single line due to a doublet species ($S = 1/2$) (Figure 7). Both signals are centered at 335 mT, $g = 2.004(1)$, typical for carbon/nitrogen-centered delocalized organic radicals. The triplet nature of the four-line spectrum is confirmed by the additional presence of a weak $\Delta m_S = \pm 2$ transition at half field (Figure 7, inset). The zero-field splitting tensor for the triplet state is nearly axial, and a least-squares analysis gives $|D| = 0.0212(2)$ cm^{-1} and $|E| = 0.0006(1)$ cm^{-1}. The intensity of the triplet spectrum decreases with decreasing temperature, confirming that the triplet is an excited state that is depopulated upon cooling. No EPR signals grow in upon cooling, which indicates that the ground state is an EPR-silent singlet. This spectrum is attributed to two antiferromagnetically coupled spins ($S_1 = S_2 = 1/2$), confirming the ligand biradical nature of **2**. From the temperature dependence of the triplet spectrum, the triplet state is significantly depopulated at 100 K (Figure S6): over 90% of spins are in the EPR-silent singlet ground state, and, consistent with this prediction, we are not able to observe EPR signals below 60 K.[26]

The triplet zero-field splitting D is determined mostly by the magnetic dipole−dipole interaction between the two unpaired spins. Assuming localized point dipoles for each spin and neglecting all quantum mechanical contributions,[27] a rough estimate of the distance r between the two spins can be obtained from $D = (3/2)(\mu_0/4\pi)g^2\beta^2r^{-3}$. The resulting distance $r \approx 5$ Å is consistent with a ligand biradical with separate delocalization of each spin over each ligand, without noticeable interligand delocalization. The value of D is similar to those obtained in other biradicals.[28,29] The triplet spectrum does not saturate under the conditions employed (up to 10 mW, 60−140 K). In contrast, the central line saturates very easily (half-saturation

dx.doi.org/10.1021/ja2015718 |J. Am. Chem. Soc. 2011, 133, 8662–8672

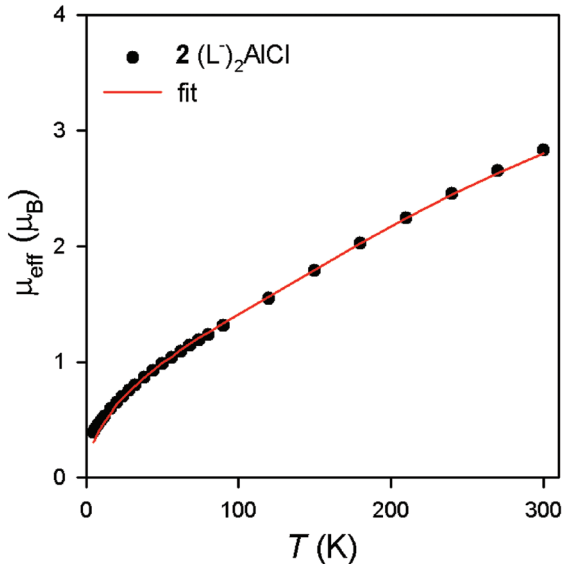

Figure 6. Magnetic susceptibility data for compound **2** in an applied field of 0.1 T. The "●" represent the experimental data, and the red "—" represents a fit to the data for **2** using a spin Hamiltonian of the form $\hat{H} = -2J\hat{S}_{L(1)} \cdot \hat{S}_{L(2)}$. Fit parameters: $g = 2.0$, $J = -230$ cm^{-1}, and TIP = 2×10^{-3} emu.

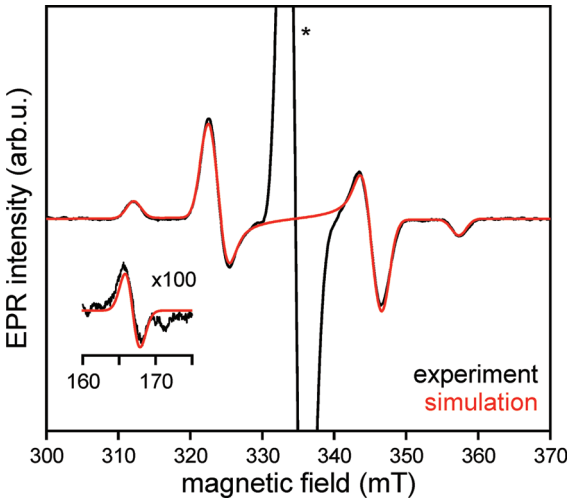

Figure 7. X-band cw EPR spectrum of a frozen solution of 1 mM **1** in 2:1 toluene:chloroform. Experimental parameters: microwave frequency 9.389 GHz, power 10 mW, temperature 100 K, modulation amplitude 1 mT. Simulation parameters: $S = 1$, $g = 2.004(1)$, $D = 0.0212(2)$ cm^{-1}, $E = 0.0006(1)$ cm^{-1}, residual peak-to-peak broadening 2.0(1) MHz. The asterisk indicates the doublet signal.

power $P_{1/2} < 10$ μW at 140 K), which is characteristic of monoradicals. In addition, the central line intensity is proportional to $1/T$ and supports the assignment to a doublet. Because of the strong saturation of the doublet signal and the strong depopulation of the triplet, it is not possible to reliably quantify the relative concentration of the two species. Moreover, the amount of monoradical varies between EPR sample preparations from the same batch of solid sample. We attribute the monoradical signal to reaction of **2** with trace amounts of dioxygen introduced during the preparation of the EPR samples and the high sensitivity of **2** toward water and dioxygen.

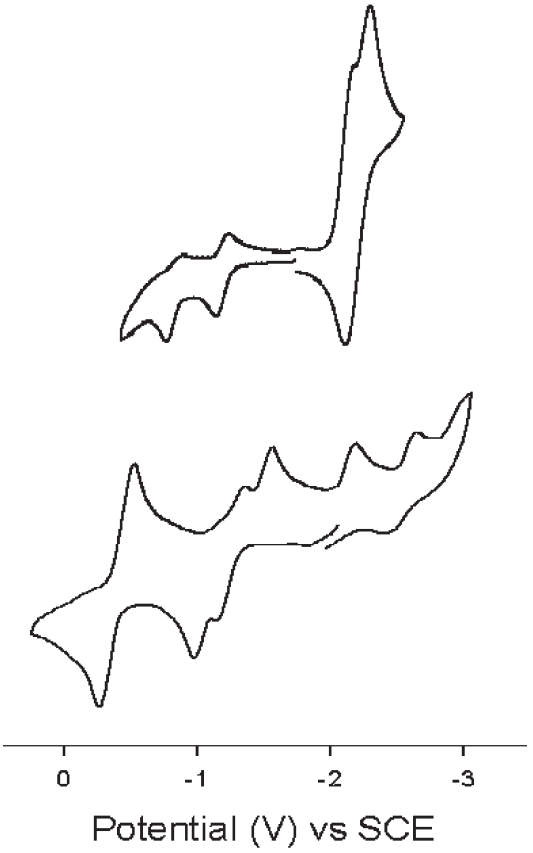

Figure 8. Cyclic voltammogram for a 1 mM solution of complex **2** (top) and of complex **5** (bottom), recorded in 0.3 M Bu_4NClO_4 THF solution.

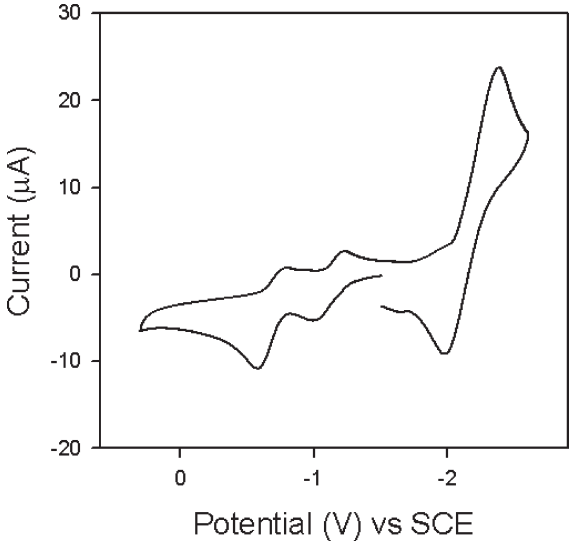

Figure 9. Cyclic voltammogram for a 1 mM solution of complex **4** recorded in 0.3 M Bu_4NClO_4 THF solution.

Electrochemical Measurements. Cyclic voltammetry measurements were obtained in 0.3 M Bu_4NClO_4 THF solutions of complexes **2**–**5** (Figures 8, 9, and S6). In most cases, the complexes gave rise to a series of four reversible redox couples corresponding to all of the expected ligand redox events, two events for each of the two ligands (Table 5).

dx.doi.org/10.1021/ja2015718 |*J. Am. Chem. Soc.* 2011, 133, 8662–8672

Table 5. Electrochemical Potentials (V vs SCE) for Ligand Reduction Events Observed in Complexes 2 and 5

		E°_{LL/LL^-}	$E^\circ_{LL^-/L^-L^-}$	ΔE°	$E^\circ_{L^-L^-/L^-L2^-}$	$E^\circ_{L^-L2^-/L2^-L2^-}$	ΔE°
2	$(IP^-)_2AlCl$	−0.86	−1.20	0.34	−2.51[a]	[b]	∼0
5	$[(IP^{2-})_2Al]^-$	−0.4[a]	[b]	∼0	−1.17	−1.36	0.19

[a] Irreversible redox event. [b] One-electron processes overlap, and so only one potential is reported.

For complex **2**, two successive one-electron oxidation events corresponding to the $IP^{0/1-}$ couple on the different ligands are observed at $E_{1/2}$ = −0.86 and −1.20 V vs SCE (Figure 8, top). The 0.34 V distance between these waves indicates that electronic coupling between the two ligands and most likely through the Al(III) center is occurring; the 0.34 V difference corresponds to a comproportionation constant, $K_c = 10^{5.8}$, for the process $(IP^-)_2AlCl + [(IP)_2AlCl]^{2+} \rightarrow 2[(IP^-)(IP)AlCl]^+$. This value is similar to those usually associated with class II mixed-valent compounds.[30] In addition, two overlapping redox couples for the two $IP^{1-/2-}$ events are observed at −2.21 V. The higher current observed in the reducing direction for this process is attributed to additional, less well-defined and irreversible ligand reduction events: we observe these irreversible reduction events between −2 and −3 V for other complexes in the $(IP^{n-})_2Al$ series even when the well-defined, reversible $IP^{1-/2-}$ couple is well-separated from them and observed at more positive potentials (for example, Figure 8, bottom). It is unlikely that these additional irreversible reduction events correspond to redox activity associated with the Al(III) center.

The redox chemistry of the mixed-valent complex **4** is somewhat less well-defined (Figure 9). Two redox couples, corresponding to successive one-electron and two-electron oxidation processes, are observed at −1.37 and −0.57 V. Presumably the first at −1.37 V involves the $IP^{1-/2-}$ couple of the IP^{2-} ligand, and the second involves concomitant $IP^{0/1-}$ couples on both of the ligands. This second couple at −0.57 V is barely reversible. At further negative potentials (−2.20 V), we observed a multielectron process, which presumably corresponds again to unidentified ligand-based, rather than metal-centered events.

It is informative to compare the voltammograms for complexes **2** and **5** (Figure 8, Table 5). Complex **5** displays a similar pattern of ligand-based redox waves as described above for complex **2**. Starting at the rest potential of −1.8 V, successive one-electron oxidation waves for the $IP^{1-/2-}$ couple on each ligand are observed at −1.36 and −1.17 V. Subsequently, a two-electron oxidation wave for the concurrent oxidation of both ligands, $IP^{0/1-}$, is observed at −0.4 V vs SCE. This concurrent oxidation is in contrast to complex **2** for which K_c for the successive ligand-based processes for $IP^{0/1-}$ was $10^{5.8}$. One possible explanation for this apparently contradictory result is the different coordination numbers and geometries of complexes **2** and **5**, which may lead to different strengths of electronic communication between the two IP ligands. Of further interest in comparing the voltammograms of **2** and **5**, the redox potentials for the $IP^{1-/2-}$ and $IP^{0/1-}$ processes in **5**, respectively, are each approximately 0.9 and 0.7 V positive of the corresponding redox couple for **2**. This shift in the redox potentials of the redox-active ligands upon removal of chloride from the coordination sphere of aluminum seems quite significant and indicates that electronic effects associated with the ligand coordination environment are transferred via the aluminum center to the iminopyridine ligands.

CONCLUSION AND OUTLOOK

We have demonstrated that redox noninnocent ligands can be employed to impart a rich redox reactivity and open shell electronic structure to the nonredox-active and strongly Lewis acidic aluminum(III) ion. Complexes of aluminum containing the neutral, monoanionic, and dianionic iminopyridine ligand have been characterized structurally and electronically. Strong antiferromagnetic coupling of ligand electrons through the aluminum center stabilizes the biradical complex $(IP^-)_2AlCl$, **2**, toward the radical ligand C−C coupling, which we observe during attempts to prepare mixed-valent doublet complexes. Moreover, we have demonstrated that electrochemical potentials are sensitive to changes in the aluminum coordination environment. Future work will focus on exploiting the unique properties obtained from the combination of ligand redox activity and an electrophilic aluminum(III) center, toward chemical transformations.

EXPERIMENTAL SECTION

Physical Measurements. Elemental analyses were performed by Columbia Analytical. ^1H NMR spectra were recorded at ambient temperature using a Varian 300 MHz spectrometer. Chemical shifts were referenced to residual solvent. Assignment of peaks in the NMR spectra of paramagnetic complexes was made wherever possible. For the most part, assignments are not given in cases where the origin of the peak was uncertain due to the paramagnetic nature of the complexes. The abbreviation py^{red} indicates reduced (and dearomatized) pyridine rings. Electrochemical measurements were recorded in a glovebox under a dinitrogen atmosphere using a CH Instruments Electrochemical Analyzer, a glassy carbon working electrode, a platinum wire auxiliary electrode, and an $Ag/AgNO_3$ nonaqueous reference electrode. Reported potentials are all referenced to the SCE couple and were determined using decamethylferrocene as an internal standard. The number of electrons passed in a given redox process was estimated by comparison of the peak current with the peak current of decamethylferrocene included as an internal standard. Magnetic measurements were recorded using a Quantum Designs MPMS XL magnetometer at 0.1 T. The sample was contained under nitrogen in a gelcap and suspended in the magnetometer in a plastic straw. The magnetic susceptibility was adjusted for diamagnetic contributions using the constitutive corrections of Pascal's constants. EPR measurements were performed on 100 μL dilute solutions of the compound loaded into 4 mm OD quartz tubes in the glovebox and then freeze−pump−thawed and flame-sealed on a Schlenk line. X-band continuous-wave EPR measurements were performed at the CalEPR center at UC Davis, with a Bruker ECS106 X-band spectrometer equipped with a Bruker SHQ resonator, an EIP 548A frequency counter, and an Oxford liquid-helium cryostat. The magnetic field was calibrated with a Bruker ER036TM teslameter. Simulations were performed with EasySpin.[31]

X-ray Structure Determinations. X-ray diffraction studies were carried out on a Bruker SMART 1000, a Bruker SMART APEXII, and a Bruker SMART APEX Duo diffractometer equipped with a CCD detector.[32a] Measurements were carried out at −175 °C using Mo Kα (λ = 0.71073 Å) radiation. Crystals were mounted on a glass capillary or Kaptan Loop with Paratone-N oil. Initial lattice parameters

dx.doi.org/10.1021/ja2015718 |J. Am. Chem. Soc. 2011, 133, 8662–8672

were obtained from a least-squares analysis of more than 100 centered reflections; these parameters were later refined against all data. Data were integrated and corrected for Lorentz polarization effects using SAINT[32b] and were corrected for absorption effects using SADABS2.3.[32c]

Space group assignments were based upon systematic absences, *E* statistics, and successful refinement of the structures. Structures were solved by direct methods with the aid of successive difference Fourier maps and were refined against all data using the SHELXTL 6.2 software package.[32d] Thermal parameters for all non-hydrogen atoms were refined anisotropically. Hydrogen atoms, where added, were assigned to ideal positions and refined using a riding model with an isotropic thermal parameter 1.2 times that of the attached carbon atom (1.5 times for methyl hydrogens).

Preparation of Compounds. All manipulations were carried out using standard Schlenk or glovebox techniques under a dinitrogen atmosphere. Unless otherwise noted, solvents were deoxygenated and dried by thorough sparging with Ar gas followed by passage through an activated alumina column. Deuterated solvents were purchased from Cambridge Isotopes Laboratories, Inc. and were degassed and stored over activated 3 Å molecular sieves prior to use. The compound 2,6-bis-(1-methylethyl)-*N*-(2-pyridinylmethylene)phenylamine[22] (abbreviated as IP) was prepared according to literature procedures. All other reagents were purchased from commercial vendors and used without further purification.

[(IP)AlCl$_3$] (***1***). $AlCl_3$ (0.13 g, 1 mmol) and IP (0.27 g, 1 mmol) were stirred in DME (5 mL) for 10 h. Hexanes (10 mL) was added to afford an orange-yellow precipitate, which was collected and washed with 5 mL of DME (0.29 g, 72%). Crystals suitable for X-ray diffraction were obtained by diffusion of ether into a CH_3CN solution of **1**. ^{1}H NMR (300 MHz, C_6D_6): 8.16 (d, J = 8.06, 2H, py), 7.63 (dd, J = 7.64, 2.93, 2H, py), 7.18 (d, J = 8.09, 2H, Ph), 6.90 (br, 1H, Ph), 5.21 (s, 1H, imCH), 3.12 (hep, J = 6.5, 1H, C*H*(CH$_3$)$_2$), 1.19 (d, J = 6.9, 6H, CH(C*H*$_3$)$_2$). Anal. Calcd for $C_{18}H_{23}AlCl_3N_2$: C, 53.95; H, 5.79; N, 6.99. Found: C, 53.82; H, 5.65; N, 6.79. UV−vis spectrum (hexanes) λ_{max} (ε_M): 238 (12 100), 348 (br, 2030) nm (L mol^{-1} cm^{-1}).

[(IP$^-$)$_2$AlCl] (***2***). Sodium metal (0.088 g, 3.85 mmol) and IP (1.0 g, 3.75 mmol) were stirred with DME (10 mL) for 1 h. The resulting deep red solution was added, dropwise, to a stirred suspension of $AlCl_3$ (0.25 g, 1.88 mmol) in DME (10 mL), and the mixture was stirred vigorously for 24 h to afford a dark green suspension. The dark green precipitate was collected, extracted into ether (4 × 20 mL), filtered through Celite, and the solvent was removed in vacuo to afford a dark green powder. A further amount of product was obtained by cooling the concentrated reaction filtrate (5 mL) at −25 °C. Yield: 0.84 g (76%) of **2**. Crystals suitable for X-ray diffraction were obtained by cooling a concentrated ether solution of **2** at −25 °C for 1 week. ^{1}H NMR (300 MHz, C_6D_6): 8.60 (br, py), 8.47 (d, J = 4.33, py), 8.29 (br, py), 7.40 (br, py), 7.05−6.63 (m), 5.21 (d, J = 8.64), 4.51 (d, J = 4.68, 2H, imCH), 4.24 (d, J = 4.53), 3.71 (m, 2H, C*H*(CH$_3$)), 1.24 (d, J = 6.59, 12H, CH(C*H*$_3$)$_2$). Anal. Calcd for $C_{36}H_{44}AlClN_4$: C, 72.64; H, 7.45; N, 9.41. Found: C, 72.10; H, 7.55; N, 9.32. UV−vis spectrum (hexanes) λ_{max} (ε_M): 242 (20 647), 358 (20 875), 706 (1818) nm (L mol^{-1} cm^{-1}). μ_{eff} = 2.8 μ_B at 300 K.

[(IP$^-$)$_2$Al(CF$_3$SO$_3$)] (***3***). Compound **3** was prepared following the same procedure described for compound **2**. However, Al(CF$_3$SO$_3$)$_3$ was used in place of $AlCl_3$. Compound **3** was obtained as a dark green powder (0.58 g, 44%). Crystals suitable for X-ray diffraction were obtained by cooling a DME solution of the product at −25 °C for 1 week. ^{1}H NMR (300 MHz, C_6D_6): 8.58 (s, py), 8.47 (d, J = 4.54, py), 8.27 (d, J = 8.64, py), 7.43 (2, py), 7.07−6.87 (m, Ph), 6.63 (s, Ph), 4.50 (s, 2H, imCH)), 4.20 (s, Ph), 3.77 (m, 2H, C*H*(CH$_3$)$_2$) 1.24 (d, J = 7.97, 12H, CH(C*H*$_3$)$_2$) ppm. Anal. Calcd for $C_{37}H_{44}AlF_3N_4O_3S$: C, 62.70; H, 6.26; N, 7.90. Found: C, 62.58; H, 6.70; N, 7.94. UV−vis spectrum (hexanes) λ_{max} (ε_M): 241 (13 610), 356 (14 940), 661 (1490) nm (L mol^{-1} cm^{-1}). μ_{eff} = 3.4 μ_B at 300 K.

[(IP^{2-})Al](μ-IP$^-$IP$^-$) (***4***). Sodium metal (0.13 g, 5.7 mmol) and IP (1.0 g, 3.75 mmol) were stirred with DME (10 mL) for 1 h. The resulting deep red solution was added, dropwise, to a stirred suspension of $AlCl_3$ (0.25 g, 1.88 mmol) in DME (10 mL), and the mixture was stirred vigorously for 36 h to afford a purple suspension. The purple precipitate was collected, extracted into ether (4 × 20 mL), filtered through Celite, and the solvent was removed in vacuo to afford a purple powder. A further amount of product was obtained by cooling the concentrated reaction filtrate (5 mL) at −25 °C. Yield: 0.56 g (55%). Crystals suitable for X-ray diffraction were obtained by cooling a concentrated ether solution of **4** at −25 °C for 1 week. ^{1}H NMR (300 MHz, C_6D_6): δ 8.60 (s, 2H, py), 8.47 (2, J = 4.56, 2H, py), 8.28 (d, J = 7.8, 2H, py), 7.42 (s, 2H, py), 6.91 (d, J = 8.9, 8H, Ph), 6.63 (t, J = 6.1, 4H, Ph), 6.14 (dd, J = 9.1, 4.8, 2H, py$_{red}$), 6.02 (d, J = 8.35 2H, py$_{red}$), 5.51 (dd, J = 8.78, 2H, py$_{red}$), 5.39 (s, 2H, imC*H*), 5.16 (d, J = 8.35, 2H, py$_{red}$), 4.46 (d, J = 6.6, 4H, C*H*(CH$_3$)$_2$), 4.19 (d, J = 7.35, 2H, (bridging imC*H*), 3.53 (hept, J = 6.75, 4H, C*H*(CH$_3$)$_2$), 1.14 (d, J = 6.9, 24H, CH(C*H*$_3$)^2) ppm. Anal. Calcd for $C_{72}H_{88}AlN_8$: C, 77.27; H, 7.92; N, 10.01. Found: C, 76.97; H, 8.19; N, 9.97. UV−vis spectrum (hexanes) λ_{max} (ε_M): 238 (6390), 356 (5300), 424 (1510) nm (L mol^{-1} cm^{-1}). This compound is diamagnetic.

[(DME)$_3$Na][(IP^{2-})$_2$Al] (***5***). Sodium metal (0.173 g, 7.5 mmol) and IP (1.0 g, 3.75 mmol) were stirred with DME (10 mL) for 1 h. The resulting deep red solution was added, dropwise, to a stirred suspension of $AlCl_3$ (0.25 g, 1.88 mmol) in DME (10 mL), and the mixture was stirred vigorously for 24 h to afford a deep purple suspension. The solvent was removed in vacuo, and the purple residue was extracted into ether (4 × 20 mL), filtered through Celite, and the solvent wasremoved in vacuo to afford **5** as a deep purple powder. A further amount of product was obtained by cooling the concentrated reaction filtrate (5 mL) at −25 °C. Yield: 0.98 g (62%). Crystals suitable for X-ray diffraction were obtained by cooling a concentrated ether solution of **5** at −25 °C for 1 week. ^{1}H NMR (300 MHz, C_6D_6): δ 7.24 (t, J = 5.05, 2H, Ph), 7.12 (d, J = 4.65 2H, Ph), 6.76 (d, J = 6.37, 2H, Ph), 5.91 (d, J = 9.6, 2H, py), 5.49 (s, 2H, imC*H*), 5.32 (dd, J = 9.1, 4.56, 2H, py), 4.65 (t, J = 5.5, 2H, py), 4.20 (hept, J = 6.7, 2H, C*H*(CH$_3$)$_2$), 2.95 (br, 12H, DME), 2.92 (br, 18H, DME), 1.48 (d, J = 7.2, 6H, CH(C*H*$_3$)^2), 1.32 (d, J = 6.1, 6H, CH(C*H*$_3$)^2) ppm. Anal. Calcd for $C_{48}H_{74}AlN_4NaO_6$: C, 67.58; H, 8.74; N, 6.57. Found: C, 66.80; H, 8.20; N, 6.79. UV−vis spectrum (hexanes) λ_{max} (ε_M): 285 (11 150), 447 (1630) nm (L mol^{-1} cm^{-1}). This compound is diamagnetic.

[(Et$_2$O)$_2$Na][(IP^{2-})$_2$Al] (***6***). Compound **6** was prepared following the same procedure described for compound **5**. However, ether was used in place of DME. Compound **6** was obtained as a purple powder (0.81 g, 59%). Crystals suitable for X-ray diffraction were obtained by cooling a DME solution of the product at −25 °C for 1 week. ^{1}H NMR (300 MHz, C_6D_6): δ 7.23 (t, J = 5.1, 2H, Ph), 7.11 (d, J = 4.6, 2H, Ph), 6.87 (d, J = 6.6, 2H, Ph), 6.58 (m, 2H, py), 5.92 (d, J = 9.3, 2H, py), 5.51 (s, 2H, im C*H*), 5.39 (m, 2H, py), 4.67 (s, 2H, py), 4.25 (hept, J = 6.6, 2H, C*H*(CH$_3$)$_2$), 1.49 (d, J = 6.8, 6H, CH(C*H*3)2), 1.39 (d, J = 6.8, 6H, CH(C*H*3)2) ppm. Anal. Calcd for $C_{44}H_{64}AlN_4NaO_2$: C, 72.30; H, 8.82; N, 7.66. Found: C, 72.08; H, 8.97; N, 7.15.

■ ASSOCIATED CONTENT

Supporting Information. CIF files for the structures of **1**−**6**, and UV−visible spectra of IP and **4**. Depictions of the solid-state structures of **1**, **3**, and **6**. Cyclic voltammogram for IP, magnetic susceptibility data for **4** and **5**, and fits to variable-temperature EPR data for **2**. This material is available free of charge via the Internet at http://pubs.acs.org.

■ AUTHOR INFORMATION

Corresponding Author
laberben@ucdavis.edu

Author Contributions

[†]These authors contributed equally.

■ ACKNOWLEDGMENT

We would like to thank the University of California, Davis for funding and Drs. J. Berg, P. Klavins, and J. Fettinger for assistance with IR spectrometer, SQUID magnetometer, and X-ray crystallography instrumentation.

■ REFERENCES

(1) *Activation of Small Molecules*; Tolman, W. B., Ed.; Wiley-VCH: Weinheim, 2006.

(2) For example: Wright, A. M.; Wu, G.; Hayton, T. W. *J. Am. Chem. Soc.* **2010**, *132*, 14336.

(3) Stephan., D. W. *Chem. Commun.* **2010**, *46*, 8526.

(4) Peng, Y.; Ellis, B. D.; Wang, X.; Fettinger, J. C.; Power, P. P. *Science* **2010**, *325*, 1668.

(5) (a) Bhugun, I.; Lexa, D.; Saveant, J.-M. *J. Phys. Chem.* **1996**, *100*, 19981–19985. (b) Bhugun, I.; Lexa, D.; Saveant, J.-M. *J. Am. Chem. Soc.* **1996**, *118*, 1769–76. (c) Hammouche, M.; Lexa, D.; Momenteau, M.; Saveant, J. M. *J. Am. Chem. Soc.* **1991**, *113*, 8455–66.

(6) Gambarotta, S.; Arena, F.; Floriani, C.; Zanazzi, P. F. *J. Am. Chem. Soc.* **1982**, *104*, 5082–92.

(7) Schmidt, M. H.; Miskelly, G. M.; Lewis, N. S. *J. Am. Chem. Soc.* **1990**, *112*, 3420–6.

(8) Menard, G.; Stephan, D. J. *J. Am. Chem. Soc.* **2010**, *132*, 1796–1797.

(9) Cui, C.; Roesky, H. W.; Schmidt, H.-G.; Noltemeyer, M.; Hao, H.; Cimpoescu, F. *Angew. Chem., Int. Ed.* **2000**, *39*, 4274.

(10) Zhu, H.; Chai, J.; Chandrasekhar, V.; Roesky, H. W.; Magull, J.; Vidovic, D.; Schmidt, H. G.; Noltemeyer, M.; Power, P. P.; Merrill, W. A. *J. Am. Chem. Soc.* **2004**, *126*, 9472–9473.

(11) (a) Herzog, S.; Geisler, K.; Praekel, H. *Angew. Chem., Int. Ed. Engl.* **1963**, *2*, 47. (b) Flamini, A.; Poli, N. *Inorg. Chim. Acta* **1988**, *150*, 149.

(12) (a) Köster, R.; Benedikt, G.; Schrötter *Angew. Chem., Int. Ed. Engl.* **1964**, *3*, 514–515. (b) Lehmkuhl, H.; Fuchs, G.; Köster, R. *Tetrahedron Lett.* **1965**, *29*, 2511.

(13) (a) Kaim, W. *J. Organomet. Chem.* **1980**, *201*, C5–C8. (b) Kaim, W. *Chem. Ber.* **1981**, *114*, 3789. (c) Kaim, W. *Z. Naturforsch.* **1982**, *37B*, 783.

(14) (a) Cloke, F. G. N.; Dalby, C. I.; Henderson, M. J.; Hitchcock, P. B.; Kennard, C. H. L.; Lamb, R. L.; Raston, C. L. *J. Chem. Soc., Chem. Commun.* **1990**, 1394–1396. (b) Cloke, F. G. N.; Dalby, C. I.; Daff, J.; Green, J. *Dalton Trans.* **1991**, 181–184.

(15) Leman, J. T.; Barron, A. R.; Ziller, J. W.; Kren, R. M. *Polyhedron* **1989**, *8*, 1909.

(16) Jurca, T.; Dawson, K.; Mallov, I.; Burchell, T.; Yap, G. P. A.; Risheson, D. S. *Dalton Trans.* **2010**, *39*, 1266.

(17) Scott, J.; Gambarotto, S.; Korobkov, I.; Knijnenburg, Q.; de Bruin, B.; Budzelaar, P. H. M. *J. Am. Chem. Soc.* **2005**, *127*, 17204.

(18) Westerhausen, M.; Bollwein, T.; Makropoulos, N.; Schneiderbauer, S.; Suter, S.; Nöth, H.; Mayer, P.; Piotrowski, H.; Polborn, K.; Pfitzner, A. *Eur. J. Inorg. Chem.* **2002**, 389–404.

(19) Lu, C. C.; Bill, E.; Weyhermüller, T.; Bothe, E.; Wieghardt, K. *J. Am. Chem. Soc.* **2008**, *130*, 3181.

(20) Wu, J. Y.; Stanzl, B. N.; Ritter, T. *J. Am. Chem. Soc.* **2010**, *132*, 13214–13216.

(21) Addison, A. W.; Rao, T. N.; Van Rijn, J. J.; Verschoor, G. C. *J. Chem. Soc., Dalton Trans.* **1984**, 1349.

(22) Laine, T. V.; Klinga, M.; Leskelä, M. *Eur. J. Inorg. Chem.* **1999**, 959.

(23) Schmitt, E. A. Ph.D. Thesis, University of Illinois at Urbana-Champaign, Urbana, IL, 1995.

(24) Ketterer, N. A.; Fan, H.; Blackmore, K. J.; Yang, X.; Ziller, J. W.; Baik, M.-H.; Heyduk, A. F. *J. Am. Chem. Soc.* **2008**, *130*, 4364.

(25) For example: (a) Crawford, V. H.; Richardson, H. W.; Wasson, J. R.; Hodgson, D. J.; Hatfield, W. E. *Inorg. Chem.* **1976**, *15*, 2107. (b) Ruiz, E.; Alemany, P.; Alvarez, S.; Cano, J. *J. Am. Chem. Soc.* **1997**, *119*, 1297.

(26) Bencini, A.; Gatteschi, D. *EPR of Exchange Coupled Systems*; Springer: Berlin, 1990.

(27) Riplinger, C.; Kao, J. P. Y.; Rosen, G. M.; Kathirvelu, V.; Eaton, G. R.; Eaton, S. S.; Kutateladze, A.; Neese, F. *J. Am. Chem. Soc.* **2009**, *131*, 10092.

(28) Gardiner, M. G.; Hanson, G. R.; Henderson, M. J.; Lee, F. C.; Raston, C. L. *Inorg. Chem.* **1994**, *33*, 2456.

(29) van Gastel, M.; Lu, C. C.; Wieghardt, K.; Lubitz, W. *Inorg. Chem.* **2009**, *48*, 2626.

(30) Robin, M. B.; Day, P. *Adv. Inorg. Chem. Radiochem.* **1967**, *10*, 247.

(31) Stoll, S.; Schweiger, A. *J. Magn. Reson.* **2006**, *178*, 42.

(32) (a) *SMART Software Users Guide, Version 5.1*; Bruker Analytical X-Ray Systems, Inc.: Madison, WI, 1999. (b) *SAINT Software Users Guide, Version 7.0*; Bruker Analytical X-Ray Systems, Inc.: Madison, WI, 1999. (c) Sheldrick, G. M. *SADABS, Version 2.03*; Bruker Analytical X-Ray Systems, Inc.: Madison, WI, 2000. (d) Sheldrick, G. M. *SHELXTL Version 6.12*; Bruker Analytical X-Ray Systems, Inc.: Madison, WI, 1999. (e) *International Tables for X-Ray Crystallography*; Kluwer Academic Publishers: Dordrecht, 1992; Vol. C.